Enhanced thermo-spin effects in iron-oxide/metal multilayers

R Ramos[1], I. Lucas[2,3,4], P. A. Algarabel[4,5], L. Morellón[2,3,4], K. Uchida[6,7,8], E. Saitoh[1,8,9,10] and M. R. Ibarra[2,3,4,11]

1. Advanced Institute for Materials Research, Tohoku University, Sendai 980-8577, Japan
2. Fundación Instituto de Nanociencia de Aragón, E-50018 Zaragoza, Spain
3. Instituto de Nanociencia de Aragón, Universidad de Zaragoza, E-50018 Zaragoza, Spain
4. Departamento de Física de la Materia Condensada, Universidad de Zaragoza, E-50009 Zaragoza, Spain
5. Instituto de Ciencia de Materiales de Aragón, Universidad de Zaragoza and Consejo Superior de Investigaciones Científicas, 50009 Zaragoza, Spain
6. National Institute for Materials Science, Tsukuba 305-0047, Japan
7. PRESTO, Japan Science and Technology Agency, Saitama 332-0012, Japan
8. Center for Spintronics Research Network, Tohoku University, Sendai 980-8577
9. Institute for Materials Research, Tohoku University, Sendai 980-8577, JapanAdvanced Science
10. Advanced Science Research Center, Japan Atomic Energy Agency, Tokai 319-1195, Japan
11. Laboratorio de Microscopías Avanzadas, Universidad de Zaragoza, E-50018 Zaragoza, Spain

Abstract

Since the discovery of the spin Seebeck effect (SSE), much attention has been devoted to the study of the interaction between heat, spin, and charge in magnetic systems. The SSE refers to the generation of a spin current upon the application of a thermal gradient and detected by means of the inverse spin Hall effect. Conversely, the spin Peltier effect (SPE) refers to the generation of a heat current as a result of a spin current induced by the spin Hall effect. Here we report a strong enhancement of both the SSE and SPE in Fe_3O_4/Pt multilayered thin films at room temperature as a result of an increased thermo-spin conversion efficiency in the multilayers. These results open the possibility to design thin film heterostructures that may boost the application of thermal spin currents in spintronics.

1. Introduction

Thermoelectric effects have been known since the discovery of the Seebeck effect (SE) [1], which is manifested as the generation of an electrical field (**E**) in a metal or semiconductor due to a thermal gradient (∇T), resulting in a conversion from heat to electricity. Large expectation of the implementation of this principle for clean energy applications has been limited by the scarce improvement of the efficiency of the thermoelectric conversion, which is described by the figure of merit $ZT = \frac{S^2 \sigma}{\kappa} T$, where T is the system temperature, $S = \frac{\vec{E}}{\nabla T}$ is the Seebeck coefficient, σ is the electrical conductivity, κ the thermal conductivity. In principle, the thermoelectric efficiency can be enhanced by simultaneously increasing σ and decreasing κ of a material. However, when κ is dominated by the electronic contribution κ_e, it is difficult to change these quantities independently in a material due to the Wideman-Franz law $\kappa_e = L\sigma T$, where L is the Lorenz number. Similar argument applies to the Peltier effect, the Onsager reciprocal of the SE, i.e. the conversion of an applied electrical field into a heat flow and described by: $\Pi = S\,T$, where Π is the Peltier coefficient. Several other approaches to improve the thermoelectric conversion performance are currently being investigated [2]. Another posible route to explore is the study of the interaction between the heat, charge, and spin degrees of freedom in magnetic materials [3, 4].
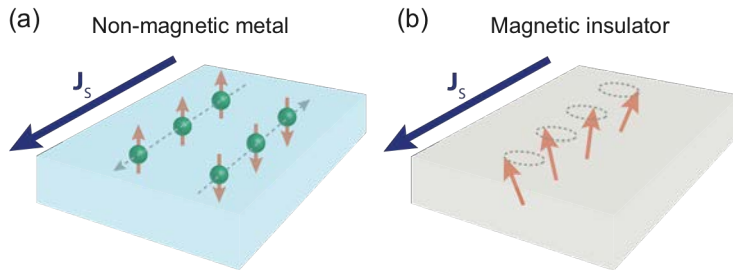

Figure 1. Schematic diagram depicting (a) conduction-electron and (b) magnon spin currents

Recently a new paradigm has gained increased attention: the generation and manipulation of spin currents (J_S) [5, 6]. This concept relies in the existence of a flow of spin angular momentum without net flow of charge. Spin currents in metals or semiconductors are originated by a net flow of the spin angular momentum of the electrons and called electron spin currents. The existence of a spin current does not necessarily imply the existence of free electrons, as in the former case, but it is also possible to have spin currents in insulating ferromagnets with localized magnetic moments [7, 8]. In this case, the magnons provide the excitation mechanism to carry spin angular momentum in the system and generate spin currents that are called magnon spin currents. (see a schematic view of both type of spin currents in figure 1).

Recent advances in this field were made possible thanks to the possibility to generate and detect these spin currents, J_S. Pioneer experiments of spin current generation were done using radiofrequency excitation in ferromagnetic materials, a phenomenon called spin-pumping [9, 10]. Subsequently, the discovery of the spin Seebeck effect (SSE) revealed that a temperature gradient in a ferromagnet (either metallic or insulator) can originate thermal spin currents [7, 11, 12, 13]. Others mechanisms, such as excitation by acoustic waves have also been demonstrated to induce spin currents in ferromagnets [14, 15, 16]. The detection of the J_S is determined by the electrical field that can induce in a metal with large

spin orbit coupling, such as Pt, adjacent to the ferromagnet, and called the inverse spin Hall effect (ISHE) [9, 17, 18, 19, 20]. More recently, the Onsager-reciprocal of the SSE has also been experimentally demonstrated, this is the spin Peltier effect (SPE) [21, 22, 23, 24, 25], which consists on the generation of a heat current as a result of a spin current injection into the ferromagnet.

This review aims to show the relevance of the thermo-spin effect in magnetic thin film multilayers of iron oxide and Pt. Here, we report the thermo-spin effect in magnetite (low electrical conductivity) and maghemite (insulator)/Pt bilayers. These are binary iron oxides crystallizing in a spinel-type structure having chemical formulae Fe_3O_4 and γ-Fe_2O_3, respectively [26, 27, 28]. The presence of additional Fe^{2+} is responsible for the moderate electrical conductivity in Fe_3O_4 [28] and magneto-resistive properties [29, 30, 31]. The study of the spin current generation in these oxide systems is interesting due to the high abundance of its constituent elements (Fe and O), the possibility of fabrication of hetero-epitaxial structures [32] and their higher Curie temperatures (848 K and 900 K for Fe_3O_4 and γ-Fe_2O_3, respectively), which could be of potential interest for thermoelectric conversion applications.

We found that the SSE is driven by the thermally generated spin currents in both iron oxides. Moreover, in $[Fe_3O_4/Pt]_n$ multilayers the SSE and SPE are strongly enhanced, which can be understood as a result of a spin current enhancement within the multilayer thickness. We also compare the thermoelectric power response of spin-Hall thermopile devices and multilayers in which we showed that the design based in the use of multilayer can achieve the largest power factor found using SSE. Finally, we briefly review the SSE in a variety of other magnetic oxides.

2. Basic mechanism and measurement procedure of thermo-spin effect:

2.1. Spin Seebeck effect (SSE)

Conventionally, the spin Seebeck effect consists on the generation of a spin current in a bilayer system comprising a ferro-, ferri-magnetic material (FM) and a normal metal (NM) via the magnetization dynamics induced by the application of a thermal gradient. The spin current injected in the NM layer is electrically detected (SSE voltage) by the inverse spin Hall effect (ISHE) as a result of the spin-orbit interaction in the NM layer (see figure 1(a)) [9, 17, 18, 19, 20]. To have a better detection efficiency, the NM is usually a heavy metal, mainly Pt [33, 34]. The ISHE-driven electric field ($\mathbf{E}_{ISHE}$) is given by the following expression:

$$\mathbf{E}_{ISHE} = \theta_{SH}\rho(\mathbf{J}_S \times \boldsymbol{\sigma}), \quad (1)$$

where θ_{SH} and ρ denote the spin Hall angle and electric resistivity of the NM layer. $\mathbf{J}_S$ and $\boldsymbol{\sigma}$ are the spatial direction of the spin current injected into NM across the FM/NM interface (parallel to ∇T) and the spin polarization (parallel to the magnetization of the FM), respectively.
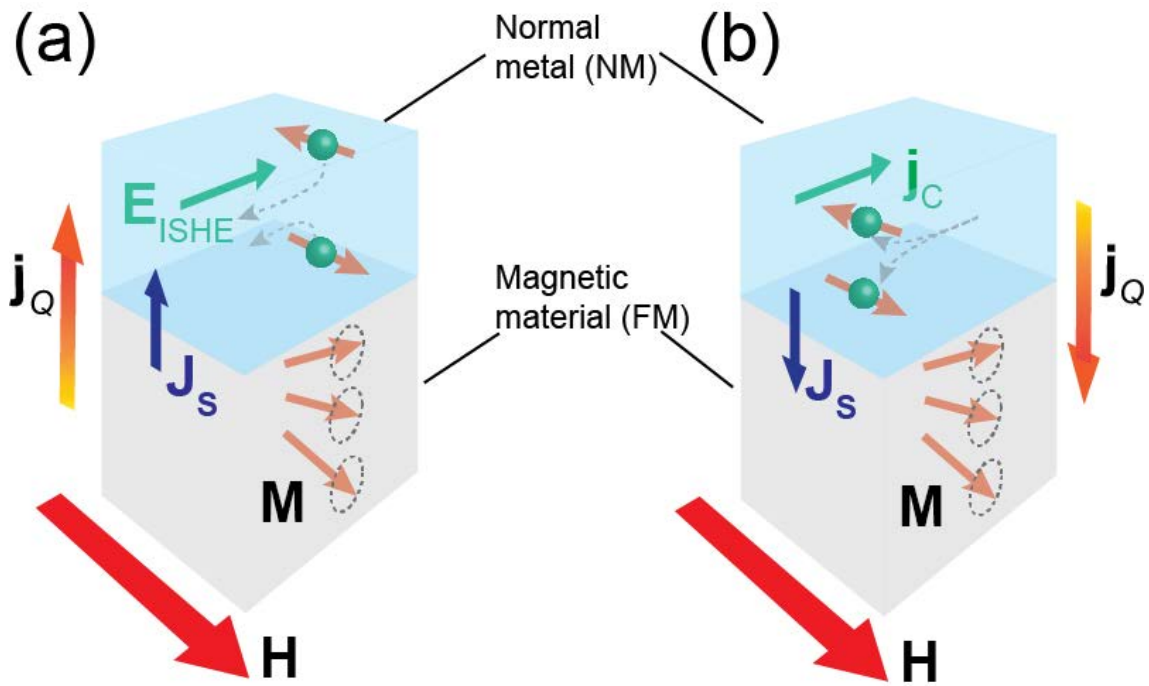
Figure 2. Schematic diagram representing the basic (a) spin Seebeck effect (SSE) and (b) spin Peltier effect (SPE) mechanism in a FM/NM bilayer with the inverse spin Hall effect (ISHE) and spin Hall effect (SHE) of the NM layer, respectively. In the SSE a thermal excitation drives a spin current while in the SPE an injected spin current induces a heat current at the FM/NM interface. The symbols: $\mathbf{E}_{ISHE}$, $\mathbf{H}$, $\mathbf{M}$, $\mathbf{j}_Q$, and $\mathbf{J}_S$ denote the ISHE-induced electric field, magnetic field, magnetization, spatial direction of heat and spin currents, respectively.

The SSE was initially observed in a $Ni_{81}Fe_{19}$ film [11], and it was theoretically formulated in terms of conduction electrons. However, the observation of the SSE in magnetic insulators pointed to its magnonic origin, due to the thermal excitation of localized spins in the ferromagnet. The theoretical framework was then developed [35, 36, 37] to explain the SSE by the thermal non-equilibrium between magnons in the FM and electrons in the NM, and the magnitude of the generated spin current was explained in terms of the difference of the effective temperatures between the magnon and electron systems. This model only considered the SSE as a result of an effective temperature difference at the interface, however experimental observations, such as the dependence of the SSE voltage on the thickness of the ferromagnet [38, 39] and its magnetic field induced suppression [39, 40, 41, 42], called for a refinement of the model. Then, Rezende et al. [43, 44] and Zhang et al. [45, 46] independently formulated the SSE by the thermally induced bulk magnon spin currents within the ferromagnet, not just at the interface. Basically, the applied heat drives the magnon system out of thermal equilibrium, thus generating a magnon accumulation. This results in the generation of a magnon spin current which is dependent on both; the applied temperature gradient and the induced magnon accumulation due to non-equilibrium magnons. Using their model several aspects of the SSE can be explained, such as the dependence on the FM thickness [38, 39], the temperature dependence [39, 43], the suppression of the SSE at high magnetic fields [39, 40, 41, 42], the multilayer SSE [47, 48, 49] (which is described below) and the observation of the SSE in antiferromagnetic materials [50, 51, 52, 53]. Other models have also been developed to explain different aspects of the SSE [54-68].

The SSE can be measured in two different experimental arrangements, these are the transverse and longitudinal SSEs, their names originate from the relative direction between the spin current and the applied temperature gradient, being perpendicular/parallel for the transverse/longitudinal SSE (see figure 3(a)/3(b)). The first experimental observation of the SSE in $Ni_{81}Fe_{19}$ was performed employing

the transverse SSE geometry, in this configuration the thermal excitation of the magnetization induces a spin current injection across the FM/NM interface, and it is detected by the ISHE in an attached Pt wire. In principle, the transverse SSE can be used to detect the SSE in magnetic materials independently of their electronic transport properties: metals, semiconductors, insulators [7, 11, 69, 70, 71]. However, this configuration is very sensitive to the thermal design of the measurement system, which can result in a voltage locally-driven by the longitudinal SSE and/or spurious voltages due to conventional spin dependent thermoelectric effects [72, 73, 74, 75].
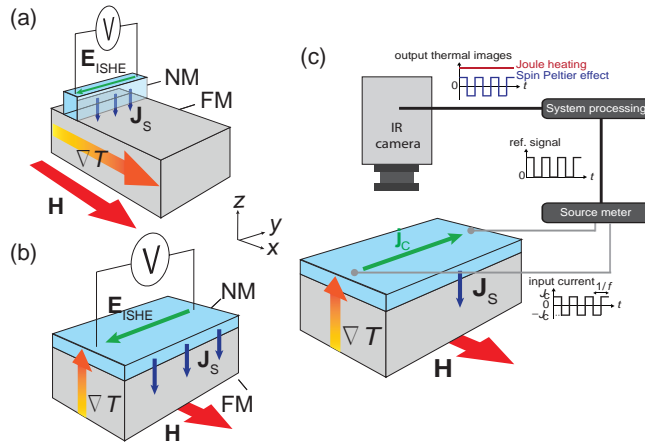

Figure 3. Schematic of the experimental configuration for the measurement of the (a) transverse, (b) longitudinal SSE and (c) thermal imaging of the SPE effect

Due to the above-mentioned complications with the transverse SSE, in this article we will focus on measurements in the longitudinal SSE (see figure 3(b)), which we will simply refer to as the SSE hereafter. Due to its simplicity, this configuration is the most commonly employed to experimentally investigate the SSE. Other possible experimental method is the non-local SSE, which is described elsewhere [76, 77, 78]. In the longitudinal SSE, the injected spin current is parallel to the thermal gradient, applied in the direction normal to the NM/FM interface, along z in figure 3(b), the magnetic field is directed in the x direction and the electric voltage detected in the y direction. This experimental configuration is similar to the one employed to measure the anomalous Nernst effect (ANE) in electrically conductive ferromagnets [79, 80, 81, 82, 83, 84, 85]. Therefore, this configuration should be ideally employed to measure the SSE of electrically insulating materials, since in conductive materials the SSE and ANE are entangled. However, we have previously shown that in ferromagnetic materials with poor electrical conductivity, the SSE dominates the spin-driven thermoelectric response due to the suppression of the ANE-driven voltage of the FM by the larger electrical conductivity of the NM layer, as described in section 3.2.1 [86].

2.2 Spin Peltier effect (SPE)

The spin Peltier effect (SPE) is the Onsager-reciprocal of the SSE, it consists on the generation of a heat current in response to a spin current injection across a FM/NM interface (parallel to the surface normal **n**) [21-25, 87, 88, 89]. The spin current is normally generated by means of the spin Hall effect (SHE) of the NM layer, such as Pt and W [33, 34], where a charge current ($\mathbf{j}_C$) induces a spin accumulation: $\boldsymbol{\mu}_S$ ($\parallel$ $\boldsymbol{\sigma}$) $\propto \theta_{SH}\mathbf{j}_C \times \mathbf{n}$ and a spin angular momentum flow (or spin current $\mathbf{j}_S$) at the FM/NM interface via the interfacial exchange coupling (see figure 1(b)). The injected spin current generates a magnon excitation in the ferrimagnet, increasing or decreasing the number of magnons depending on the relative orientation

between $\boldsymbol{\sigma}$ and $\mathbf{M}$ (parallel or antiparallel), this induces a temperature difference due to energy transfer by the spin current injection at the FM/NM interface, which can be understood by the following relation:

$$\Delta T_{SPE} \propto \boldsymbol{\mu}_S \cdot \mathbf{m} \propto (\mathbf{j}_C \times \mathbf{n}) \cdot \mathbf{m}, \qquad (2)$$

For a more detailed theoretical description of the SPE, the reader is referred to the recently developed theoretical models [87, 88, 89].

The SPE-driven temperature difference in FM/NM junctions has been detected by means of two different experimental methods: thermocouple sensors [21, 25] and lock-in thermography [22, 23, 24]. In this paper, we review measurements performed using the lock-in thermography method [90, 91]. Here, the infrared thermal radiation emitted from the sample surface is measured by an infrared (IR) camera while a rectangular wave charge current with amplitude J_C, frequency f is applied to the Pt layer of the samples in the y direction, and an in-plane magnetic field $\mathbf{H}$ with magnitude H is applied in the x direction (see figure 3(c)). The obtained thermal images are transformed into the lock-in amplitude A ($A > 0$) and phase ϕ ($0 < \phi < 360$) images by Fourier analysis. By extracting the first harmonic response of the thermal images the contributions from the SPE (time varying response) ($\propto J_C$) and Joule-heating (constant in time) ($\propto J_C^2$) can be separated. The detected IR intensity is converted into temperature information following the calibration method detailed in the supplementary information of [22].

3. Spin Seebeck effect in Fe-based binary spinel oxides:

3.1 γ-Fe$_2$O$_3$/Pt system

We have investigated the SSE of γ-Fe$_2$O$_3$, an electrical insulator with a band gap of ~ 2.0 eV [26]. Both γ-Fe$_2$O$_3$ and Fe$_3$O$_4$ have similar crystal structures, with the difference that only Fe^{3+} cations are present in γ-Fe$_2$O$_3$ and charge neutrality is achieved by the presence of cation vacancies in the octahedral sites [26]. γ-Fe$_2$O$_3$ is a well-known ferrimagnetic material with a high Curie temperature ~ 900 K, which has been used in magnetic recording technologies [27].

The films shown here were obtained by in-situ oxygen annealing of Fe$_3$O$_4$ films, previously deposited by pulsed laser deposition (PLD), for 2.5 h under different oxygen partial pressures. Figures 4(a) and 4(b) show the results of the X-ray diffraction and temperature dependence of the magnetization, respectively. After oxygen annealing, the (004) peak reflection shifts to a higher angle with a value in reasonable agreement to that of γ-Fe$_2$O$_3$. Moreover, the Verwey transition [28] observed in magnetization measurements for Fe$_3$O$_4$ film (figure 4(b)) disappears upon oxygen annealing, as expected. For more details about sample fabrication procedure and characterization see Ref. [92].

The results of the SSE measurements are shown in figure 5(c), we can see that the magnitude of the measured voltage is quite similar for all the samples, with a slight increase for the sample annealed under higher oxygen partial pressure. This result suggests that both oxide films possess similar spin current generation properties [92, 93], therefore in the rest of this review we will focus on the results obtained in bilayers and multilayers based on Fe$_3$O$_4$ due to the simplicity of sample preparation.
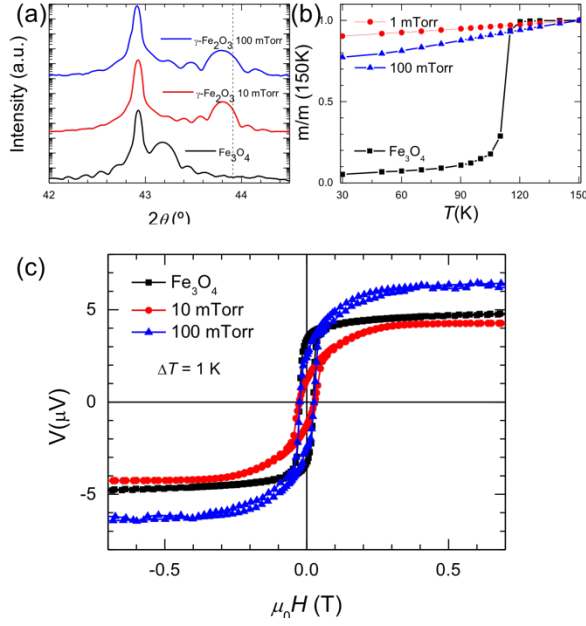
Figure 4. (a) X-ray diffraction patterns around the MgO(002) reflection showing the (004) reflections for Fe_3O_4 and $\gamma\text{-}Fe_2O_3$ under different oxygen annealing pressures. The dashed line shows the expected (004) reflection of $\gamma\text{-}Fe_2O_3$ after considering a constant volume unit cell. (b) Temperature dependence of the magnetization measured under a constant external magnetic field $\mu_0H = 0.05$ T (characteristic Verwey transition at $T \sim 110$ K is present for Fe_3O_4 film [28]). (c) SSE-induced voltage for Fe3O4 and $\gamma\text{-}Fe_2O_3$ annealed under different oxygen partial pressures. The thickness of the iron oxides is 60 nm and the Pt thickness is 7 nm. Adapted from Jiménez-Cavero *et al.* [92].

3.2 Fe_3O_4/Pt system

3.2.1 Bilayers

As previously discussed, the SSE in the longitudinal configuration and the ANE share the same experimental geometry. The ANE induced electric field ($\mathbf{E}_{ANE}$) is given by:

$$\mathbf{E}_{ANE} = Q_{ANE}\mu_0(\nabla T \times \mathbf{M}), \qquad (3)$$

were $Q_{ANE}, \mu_0, \nabla T$, and $\mathbf{M}$ are the ANE coefficient, vacuum permeability, applied thermal gradient and magnetization of the sample, respectively. We can see that this expression has a clear resemblance to that of the ISHE-induced electric field in an in-plane magnetized (IM) configuration (see equation (1)). Therefore, when measuring the SSE in non-insulating ferromagnets, the contributions from ANE and SSE can be entangled [94, 95, 96]. However, we have previously shown that, when the electrical conductivity of the ferromagnet is comparatively lower than that of the normal metal, the SSE dominates the transverse thermoelectric voltage response, as a consequence of the suppression of the ANE voltage of the ferromagnet by the larger electrical conductivity of the NM layer [86]. Since Fe_3O_4 has a moderate electrical conductivity due to electron hopping between the octahedral-coordinated Fe cations due to their mixed electronic valences (equal number of Fe^{2+} and Fe^{3+}) [28], an ANE-driven transverse thermoelectric voltage response is present [84]. However, due to the electrical resistivity of Fe_3O_4 ($\rho_{Fe3O4} = 6.94\times10^{-5}$ Ωm) being about two-orders of magnitude larger than that of Pt ($\rho_{Pt} = 1.39\times10^{-7}$ Ωm), in the Fe_3O_4/Pt junction system the contribution from the ANE of Fe_3O_4 to the transverse thermoelectric voltage is strongly suppressed. We have measured the ANE and SSE in Fe_3O_4 layer and Fe_3O_4/Pt bilayers (see figure 5) with thicknesses $t_{Fe3O4} = 34$ nm and $t_{Pt} = 17$ nm, and found that the ANE

is strongly suppressed with the SSE giving the dominant contribution to the transverse thermoelectric voltage in the Fe_3O_4/Pt system [85]. More details about sample preparation can be found elsewhere [47].
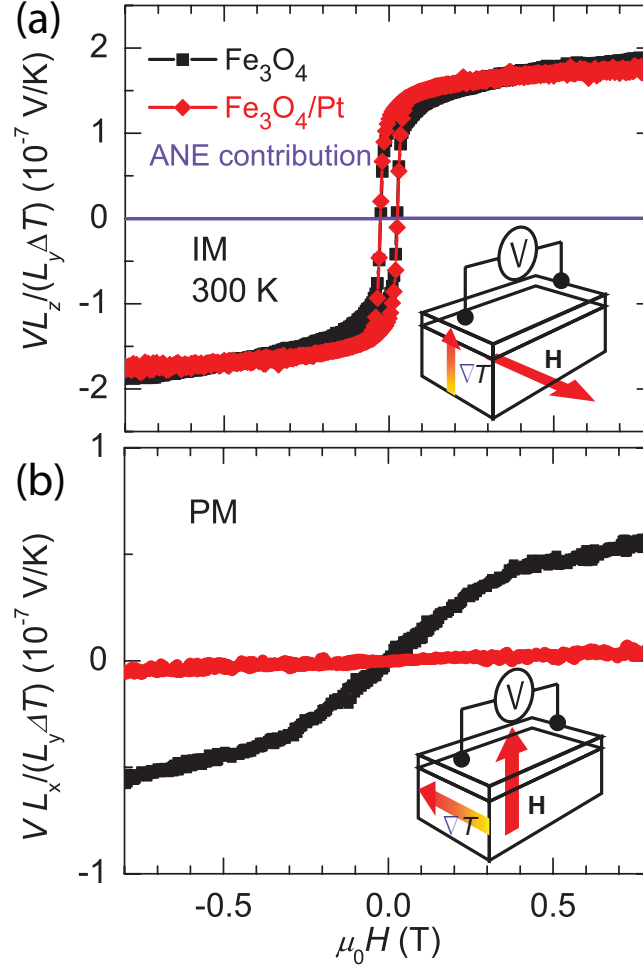

Figure 5. Transverse thermoelectric voltage measured at 300 K in the (a) in-plane magnetized (IM) and (b) perpendicular magnetized (PM) configuration on a MgO(001)//Fe_3O_4(34) and MgO(001)//Fe_3O_4(34)/Pt(17)SSE heteroepitaxial thin films (thickness in nm).The insets show the experimental geometry configuration in each case. The purple line in (a) indicates the estimated contribution from the ANE of the Fe_3O_4 layer in the Fe_3O_4/Pt sample after considering the effect of shunting of Pt in equation 5. Adapted from Ramos *et al.* [47]

The amount of ANE suppression can be estimated by considering the expression of the charge current density (J^i_m) under applied electric fields (E^j) and thermal gradients ($\nabla_k T$) in the linear response region: $J^i_m = \sigma^{ij}_m E^j - \alpha^{ik}_m \nabla_k T$, where σ^{ij}_m and α^{ik}_m are the elements of the electric and thermoelectric conductivity tensors, respectively. This expression can be expanded, under the conditions of the SSE in a FM/NM bilayer, to obtain the following relations:

$$J^z_{FM} = \sigma^{zz}_{FM} E^z + \sigma^{zy}_{FM} E^y - \alpha^{zz}_{FM} (\nabla_z T)_{FM},$$
$$J^y_{FM} = \sigma^{yz}_{FM} E^z + \sigma^{yy}_{FM} E^y - \alpha^{zy}_{FM} (\nabla_z T)_{FM},$$
$$J^z_{NM} = \sigma^{zz}_{NM} E^z - \alpha^{zz}_{NM} (\nabla_z T)_{NM},$$
$$J^y_{NM} = \sigma^{yy}_{NM} E^y. \tag{4}$$

The SSE measurement is performed in open circuit condition: $I^z = AJ^z_{FM} = AJ^z_{NM} = 0$ and $I^y = S_{FM}J^y_{FM} + S_{NM}J^y_{NM} = 0$, where $A = L_x L_y$ is the area of the junction normal to the film surface and $S_m = L_x t_m$ is the area along the y direction, where t_m (m: FM, NM) represents the thickness of each of the layers of the

FM/NM bilayer. Solving equation (4) with the open circuit condition, we obtain the following expression for the electric field in the normal metal due to the ANE of the ferromagnet [86]:

$$E^y = r/(1+r)\, E_{ANE} \qquad (5)$$

where $r = (\rho_{NM}/\rho_{FM})(t_{FM}/t_{NM})$ accounts for the degree of suppression of the ANE electric field from the FM layer by the NM layer (shunting factor), with $\rho_{FM/NM} = 1/\sigma_{FM/NM}$ being the electrical resistivity of the FM/NM layer. Considering the values of resistivity and thickness for the films in the Fe_3O_4/Pt bilayers, we can estimate the voltage contribution from the ANE of the Fe_3O_4 film, accounting for about 0.4 % of the SSE voltage measured in the Fe_3O_4/Pt bilayer (see figure 5(a)), clearly showing that the transversal thermoelectric voltage in this system is mainly driven by the SSE effect. Moreover, we measured the ANE in the perpendicular magnetized (PM) configuration, performed by interchanging the directions of ∇T (|| x) and $\mathbf{H}$ (|| z) (see inset of figure 5(b)). In this configuration only the ANE is present, since the SSE cannot be detected due to the ISHE geometry: $\mathbf{s} \parallel \mathbf{J}_S \parallel z$ due to $\mathbf{M} \parallel z$, see equation 1. The result shows that the ANE in the Fe_3O_4/Pt bilayer is negligible (see figure 5(b)), this is in agreement with a dominant SSE thermoelectric response in Fe_3O_4/Pt junction systems.

3.2.2 Multilayers

We have previously studied multilayers formed by repeated growth of [Fe_3O_4/Pt] bilayer structures as schematically depicted in figure 6(a). We have observed that in the multilayers is possible to obtain both an enhancement of the SSE voltage (see figure 6(b)) and reduction of device resistance [47], therefore achieving improved thermoelectric power output characteristics in this type of systems [48]. The reduction of the multilayer resistance is expected, since the system can be understood as a set of thin film layers electrically connected in parallel. However, the observed voltage enhancement is quite surprising and cannot be explained by a simple picture of thermal spin injection at the FM/NM interface. In this picture, the multilayer is treated as a set of independent Fe_3O_4/Pt bilayers connected in parallel with a constant heat flow, and therefore the magnitude of the injected spin currents at the Fe_3O_4/Pt interfaces considered to be constant (see figure 6(d)), then a voltage enhancement is only expected for the inner Pt layers due to additive spin current injection from both top and bottom Fe_3O_4/Pt interfaces. In the limiting case of a multilayer consisting of a very large number of bilayers, the maximum expected voltage in this scenario would be $V \approx 2\, V_{BL}$ (where V_{BL} refers to the SSE voltage of a single Fe_3O_4/Pt bilayer).
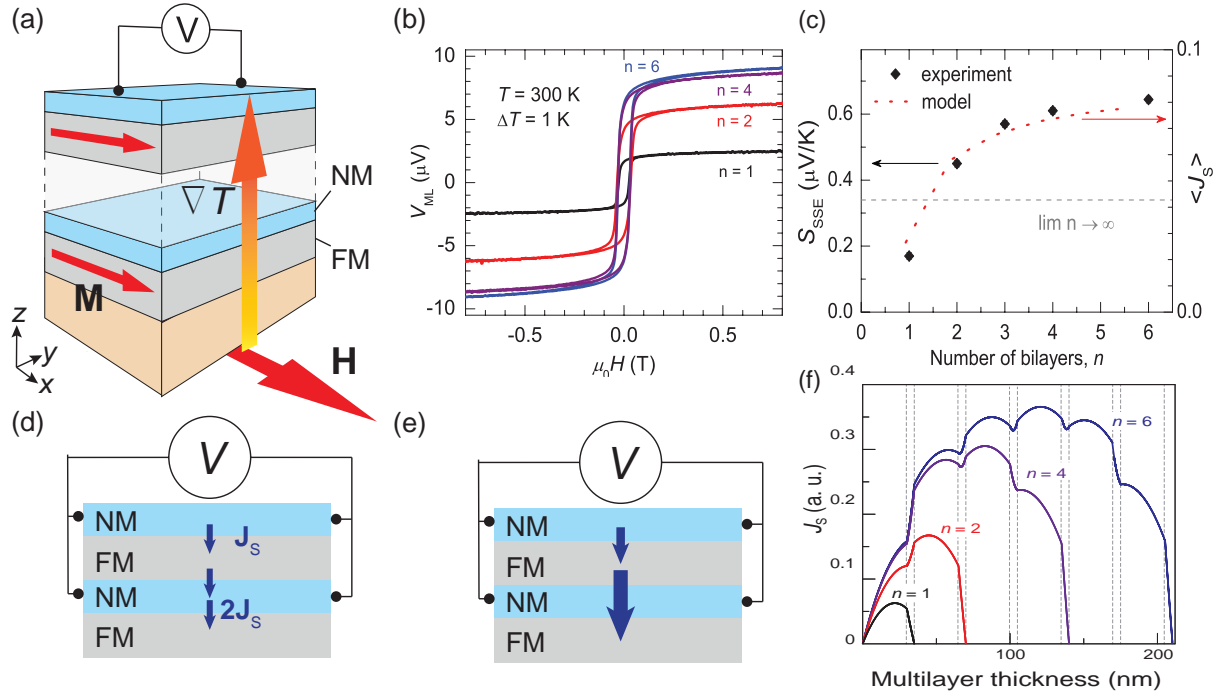
Figure 6. (a) Schematic representation of the multilayer structures for the SSE measurements. (b) Magnetic field dependence of the SSE voltage measured at 300 K for the $[Fe_3O_4(34)/Pt(17)]_n$ multilayers for different number of bilayers n (thickness in nm) and (c) the n dependence of the SSE coefficient obtained from the SSE voltage value at 0.7 T ($S_{SSE} = (V_{ML}(0.7)/\Delta T)(L_z/L_y)$). The red dot line shows the qualitative comparison to the theoretical model of the multilayer SSE and the grey dashed line shows the expected maximum enhancement from (d) a simple thermal spin current injection picture in multilayers. (e) Schematic representation of the spin current enhancement in the FM/NM multilayer system (size of arrow proportional to spin current magnitude and (f) spin current profile across the multilayer from our theoretical model. Adapted from Ramos *et al.* [47]

Figure 6(b) shows the magnetic field dependence of the SSE voltage of a set of $[Fe_3O_4/Pt]_n$ multilayers measured at room temperature, it can be observed that the voltage increases significantly upon increasing the number of bilayers n, with more than a 4× increase between a single bilayer (n=1) and a multilayer with n = 6. This is quite unexpected and clearly exceeds the maximum expected value ($V \approx 2 V_{BL}$, for n→∞) considering the simple picture described above. Figure 6(c) shows the measured SSE coefficient (defined as $S_{SSE} = (V_{ML}/\Delta T)/(L_z/L_y)$) obtained from the saturating field value for the different multilayers, we can see that even for n = 2 the measured voltage clearly exceeds $2 V_{BL}$. Similar voltage enhancements have been also reported in other multilayer systems based on all-metal [94, 95] and all-oxide layers [97], however in these systems the contributions from ANE and SSE cannot be easily separated, due to the similar resistivities of the FM and NM layers.

Now, let us discuss the different possibilities behind the observed SSE enhancement in the multilayers. One possibility could be a decrease of the thermal conductivity in the multilayers due to the increased number of interfaces, however thermal transport measurements in the $[Fe_3O_4/Pt]_n$ multilayers have shown an almost independent value of the thermal conductivity with the number of Fe_3O_4/Pt interfaces [47], suggesting that other mechanism must be responsible for the observed SSE voltage enhancement. Another possibility is the modulation of the spin transport across the multilayer thickness. To further explore this possibility, the effect of a spin current suppression in the multilayers was studied. This was performed by replacing the inner Pt interlayers of the sample for thick MgO layers, leaving only the topmost Pt layer, therefore heat transport across the multilayer thickness was maintained (MgO is a good thermal conductor), while the electron and spin transport across the multilayer thickness is suppressed. The results of this measurement are shown in figure 7, where the measured SSE voltages

of a Fe_3O_4/Pt bilayer, a $[Fe_3O_4/Pt]_3$ multilayer and a $[Fe_3O_4/MgO]_2/Fe_3O_4$/Pt multilayer are compared. The SSE voltage shows a strong suppression upon insertion of MgO interlayers, as a consequence of the absence of spin current propagation through the MgO interlayers, the obtained SSE voltage is comparable to that of a single Fe_3O_4/Pt bilayer. This result points to the spin transport across the multilayer thickness as the possible origin for the observed SSE enhancement, in which the existence of multiple Fe_3O_4/Pt interfaces is a relevant factor.
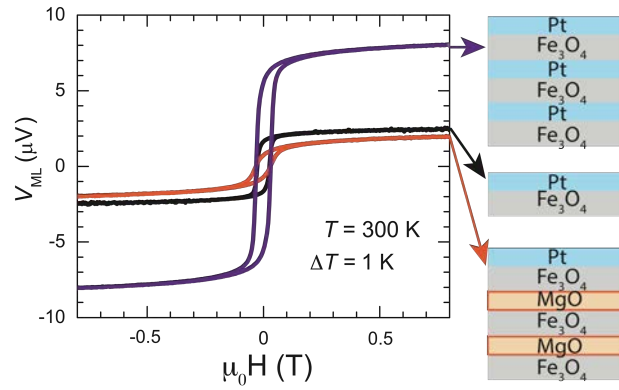

Figure 7. Effect of insertion of an electrically insulating 8nm thick MgO layer between the Fe_3O_4 layers, only the topmost Pt layer is kept for the detection of the SSE on the multilayer SSE. The samples compared are a Fe_3O_4/Pt bilayer, a $[Fe_3O_4/Pt]_3$ and a $[Fe_3O_4/MgO]_2/Fe_3O_4$/Pt multilayers. The layer thicknesses are 34 and 17 nm for Fe_3O_4 and Pt, respectively. Adapted from Ramos *et al.* [47]

Now let us briefly introduce the details of the model used to qualitatively explain the physics behind the SSE voltage enhancement in $[FM/NM]_n$ multilayers. In this model, two types of spin currents are considered: magnon spin currents (J_M) in the FM layers [8, 43, 44, 45, 46] and conduction-electron spin currents in the NM layers (J_S). Then, we consider boundary conditions for the spin current propagating across the FM/NM interfaces: continuity of the magnon and conduction-electron spin currents at the different FM/NM (NM/FM) interfaces of the multilayer [43, 44, 45, 46, 98] and the cancellation of the magnon and conduction-electron spin currents at the bottom and top surfaces of the multilayer structure. The above conditions result in a modification of the magnitude and spatial profile of the spin current: the continuous and non-vanishing spin current at the inner FM/NM interfaces of the multilayer results in an enhancement of the spin current, with maximum values at the inner layers of the multilayer (see the supplementary information of Ref. [47] for a detailed discussion). A schematic of the predicted spin current profile using our model is shown in figure 6(f), the effect can be understood by the appearance of a new length scale that characterizes the overall variation of the spin current in the multilayer, and the presence of NM layers within the multilayer that electrically detect the large spin currents at the inner layers of the multilayer. The effectively measured SSE is an average over all the NM layers, due to the parallel contact between all the layers, and thus proportional to the average spin current over all the NM layers ($<J_S>$). The predicted values of the average spin current are shown in figure 6(c), we can clearly see that the model qualitatively reproduces the observed dependence of the SSE on the number of bilayers n.

4. Spin Peltier effect in Fe-based binary spinel oxides: Fe_3O_4/Pt system

As described previously, the SPE refers to the generation of a heat current as a result of a spin current injected across the NM/FM interface. The spin current is normally generated by means of the spin Hall

effect in the NM layer [33, 34], which induces a spin accumulation near the NM/FM interface and thus injects a spin current into the FM layer.

In this section, we will discuss the results of the spin Peltier measurements in the $[Fe_3O_4/Pt]_n$ systems using the lock-in thermography (LIT) technique, reported in [23]. Let us first describe the phenomenological behavior of the SPE in the LIT measurements with focusing on the results obtained for the n = 6 multilayer system. Figures 8(a) and 8(b) show the amplitude (A) and phase (ϕ) images for a magnetic field of $\mu_0 H = 1$ T applied along the +x direction, we can see a clear temperature modulation appearing with a phase of $\phi = 0°$. Interestingly, upon reversal of the applied magnetic field direction (**H** || -x), the phase changes by 180°, while the magnitude of A remains constant (figures 8(c) and 8(d)). Figures 8(e) and 8(f) show the comparison of the magnetic field dependence of A and ϕ to the magnetization of the n = 6 sample, respectively. It can be clearly seen that the magnitude of A traces the magnetization of the sample and that the sign of the current-induced temperature modulation on the sample surface is reversed (180° phase shift) upon reversal of the magnetization of the sample. This result is consistent with the expected behavior of the SPE, thus confirming the spin origin of the measured temperature modulation, further details can be found in Ref. [23].
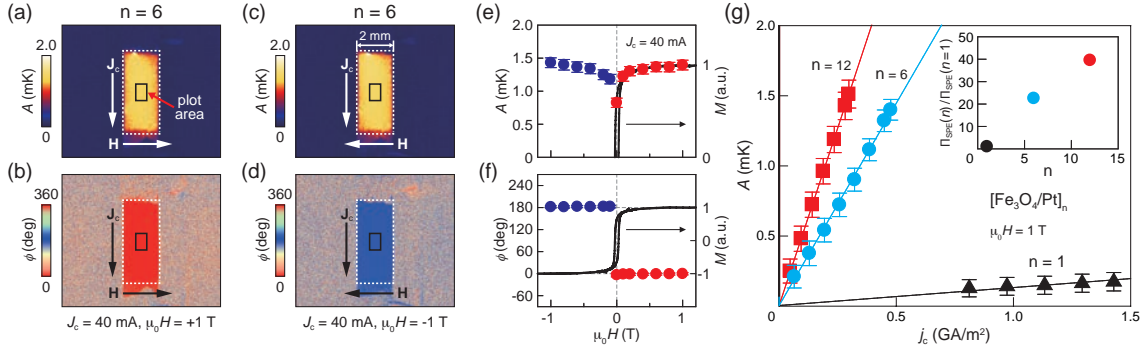

Figure 8. (a) and (b) Amplitude *A* and phase *f* images of the lock-in thermography measurements for the $[Fe_3O_4(23)/Pt(7)]_6$ sample (thickness in nm). (c) and (d) show the *A* and *f* measured upon reversal of the magnetic field direction. (e) and (f) Comparison of the magnetic field dependence of *A* and *f* to the magnetization of the sample. (g) Dependence of A on the applied charge current density for n = 1, 6 and 12. The inset shows the n dependence of the SPE enhancement ($\Pi_{SPE}(n)/\Pi_{SPE}(1)$), where $\Pi_{SPE}(n)$ is given by the slope of the curves for each n. Adapted from Uchida *et al.* [23].

Now let us move to the dependence of the SPE magnitude on the number of bilayers n. We can clearly observe a dramatic increase in the magnitude of *A* with an increasing number of bilayers n. In figure 8(g) the dependence of the SPE with the magnitude of the applied electric current density (j_c) is also shown for three different samples (n = 1, 6 and 12), showing a linear dependence (consistent with the characteristics of the SPE). The slope of these curves gives the SPE magnitude per charge current density (Π_{SPE}) as a function of number of bilayers n. This is shown in the inset of figure 9(g) after normalizing vs the value for n =1, which gives the enhancement factor of the SPE ($\Pi_{SPE}(n)/ \Pi_{SPE}(1)$). A strong increase, reaching a factor of 40 for n = 12, is observed. The observed SPE enhancement cannot be explained by considering the multilayers as stacks of independent Fe_3O_4/Pt bilayers, which gives an enhancement ratio of only 23 (proportional to the number of interfaces 2n-1). The observed unconventional enhancement can be explained using a mechanism similar to that used for the multilayer SSE [47], consisting on a redistribution of the magnon and electron spin currents across the multilayer thickness as described in the previous section. These results demonstrate the reciprocity of the SSE and SPE in multilayer systems and pave the way for realization of spin-current-based thermoelectric conversion devices.

5. Towards improved SSE thermoelectric conversion:

5.1 Common approaches

The SSE has potential advantages over conventional thermoelectric conversion technologies for heat energy harvesting or sensing applications due to its observation in magnetic insulators [4]. Moreover, the experimental geometry, with independent and perpendicular paths for the heat and electric currents, allows to have two materials that can be optimized independently and easy implementation of thin film and flexible devices over large surfaces by thin film coating [99, 100]. However, one obstacle for the implementation of thermoelectric conversion devices based on the SSE is the low magnitude of the SSE thermopower. Several approaches are currently being explored in this direction [12]; these include increasing the spin-current detection efficiency by using metallic layers with improved spin Hall angle characteristics [101, 102, 103], spin momentum locking in topological insulators [104, 105], hybrid ANE/SSE thermoelectric generation in thin films or bulk composite systems [96, 106, 107, 108], spin Hall thermopiles (figure 10(a)) [40, 109], and [FM/NM]$_n$ multilayers [23, 47, 48, 49, 94, 95, 97].

The spin Hall thermopiles improve the electrical detection of the SSE by enhancing the SSE voltage. This is achieved by using two different materials with different spin Hall angles, that are alternatively placed on top of a ferromagnetic material connected in series forming a zig-zag structure (see figure 9(a)) [48, 109]. Figure 9(b) shows the comparison of the SSE thermoelectric voltage response between a single Fe_3O_4/Pt bilayer and a spin Hall thermopile comprising a set of 6 parallel Fe_3O_4/Pt wires connected in series forming a zig-zag structure using a metal with negligible spin Hall angle (130 nm of Al) (see inset of figure 9(a) for an optical image). We observe a clear enhancement of the SSE voltage in the thermopile structure with thermoelectric voltages of 10 µV/K and 50 µV/K for the single bilayer and thermopile structure, respectively. In the zig-zag structure, the estimated SSE voltage per Fe_3O_4/Pt wire is ~ 8.2 µV/K, obtaining a value of the electric field per unit of temperature difference $V/L_y\Delta T$ ~ 1.6 mV/Km, which is consistent with the electric field of the Fe_3O_4/Pt bilayer, therefore implying that the larger SSE voltage in the thermopile is a consequence of an increased effective length of the sample and that further enhancements can be obtained by increasing the wire integration density of the devices [109]. Despite the increase of the SSE voltage in the spin Hall thermopile devices, the output power, obtained by measuring the SSE voltage on a resistive load (R_L) attached to the SSE device (inset of figure 9(c)), shows no improvement when compared to the single bilayer case (figure 9(c)). This situation arises as a consequence of the fact that, in the thermopile structures, the effective device area is reduced in the patterned device and the voltage enhancement is due to the increase in effective length of the sample, resulting in an increase of the internal resistance of the thermopile [13], which strongly limits the extractable power of these devices.
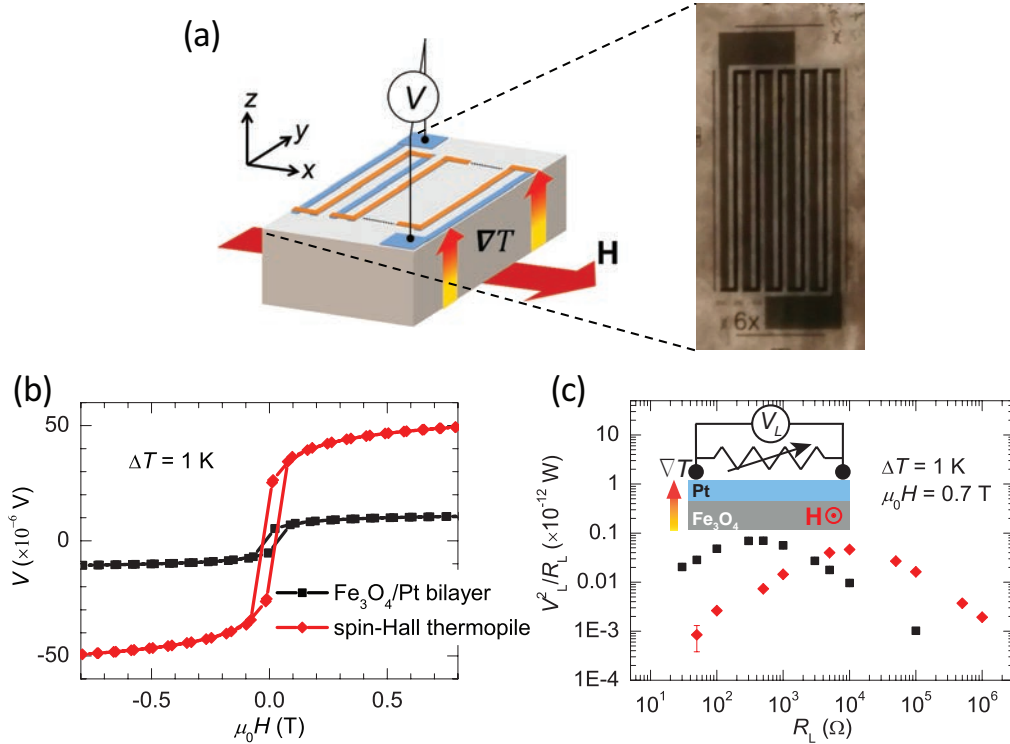
Figure 9. Illustration of the SSE measurement in a (a) spin Hall thermopile system (the optical image shows a Fe_3O_4/Pt thermopile with Al(130) interconnecting wires. (b) Magnetic field dependence of the SSE voltage measured at 300 K and with an applied temperature difference of ΔT = 1 K in a Fe_3O_4(50)/Pt(5) and a spin Hall thermopile fabricated on the same bilayer (thickness in nm). (c) Thermoelectric power output characteristics of the bilayer and the spin Hall thermopile structures measured as a function of the magnitude of a variable load resistance (R_L) connected to the device under test (see inset). Adapted from Ramos *et al.* [48]

5.2 Our approach: $[Fe_3O_4/Pt]_n$ multilayer

We have seen that the SSE-driven thermoelectric voltage in $[Fe_3O_4/Pt]_n$ multilayers is strongly enhanced as a consequence of a possible spin-current increase within the multilayers. In fact, a reduction of the Pt thickness results in a larger SSE voltage (see figure 10(a)). Moreover, in the multilayer system, the voltage increase is accompanied by a reduction of the sample resistance, thus an increase of the extractable thermoelectric power from the device is expected. We estimated the deliverable thermoelectric power of the $[Fe_3O_4/Pt]_n$ multilayers by performing measurements of the voltage on a variable resistive load connected to the multilayers, as previously done for the thermopile structures (inset of figure 9(c)). Figure 10(b) shows that the output power characteristics of the $[Fe_3O_4/Pt]_n$ multilayers are largely improved, with an enhancement of more than two orders of magnitude from the single bilayer (n = 1) to the multilayer with n = 12. This result demonstrates that the overall thermoelectric performance of the multilayers has clear advantages with respect to a single FM/NM bilayer and spin Hall thermopile structures.

According to the multilayer SSE model, the enhancement of the SSE in multilayers is expected to be strongly dependent on the spin transport characteristics in FM and PM layers, as we have observed in temperature dependent measurements [49]. Here, an increase of the multilayer enhancement ratio was observed to increase with decreasing the temperature, in agreement with larger characteristic lengths for spin transport in Fe_3O_4 and Pt at lower temperatures [93, 110]. This result suggests that there is room for further improvement of the multilayer SSE performance by selection of materials with better spin transport characteristics.
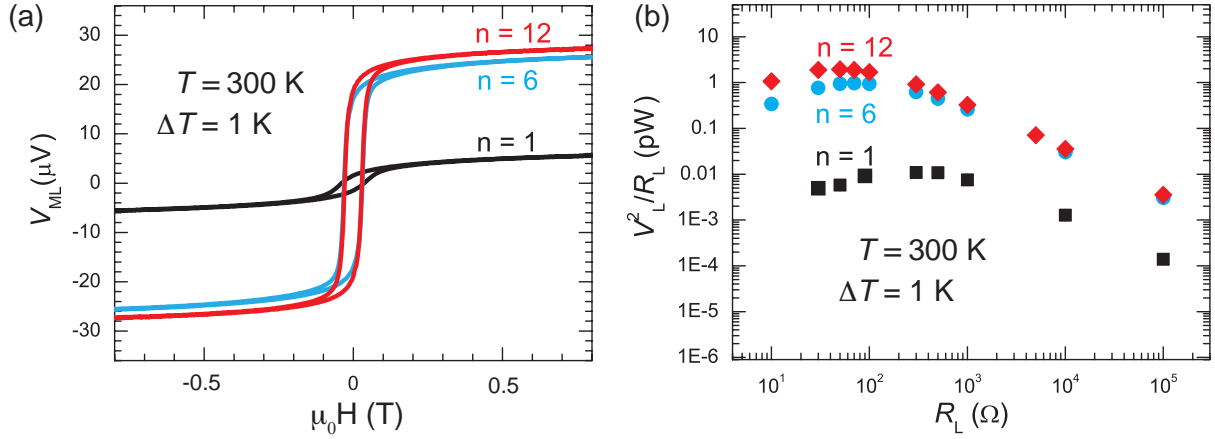
Figure 10 (a) Magnetic field dependence of the SSE voltage in [Fe$_3$O$_4$(23)/Pt(7)]$_n$ multilayers with n = 1, 6 and 12 (thickness in nm) and their (c) thermoelectric power output characteristics determined from the voltage measured on a variable load resistance as shown in the inset of figure 10(d) (figure shows values estimated from SSE voltage at *H* = 0.7 T). Adapted from Ramos *et al.* [48]

6. Spin Seebeck effects in other magnetically-ordered materials.

In the previous sections, we have described the SSE in FM/NM-based bilayer and multilayer systems, where FM is a ferro- or ferri-magnet material, and NM is a normal metal (NM). More recently, heat driven spin currents by the SSE have been observed in a wider range of materials presenting different types of magnetically ordered arrangements, these include: compensated ferrimagnets, antiferromagnets, paramagnets, systems with frustrated magnetic order and amorphous materials [50, 51, 111, 112, 113, 114]. In this section, we will briefly provide an overview of these recent developments.

As previously shown in section 2.1, the SSE was initially formulated in terms of conduction electrons [11], however with the observation of the SSE in magnetic insulators the theoretical framework was reformulated in terms of temperature differences between the magnon and electron systems in FM and PM, respectively [35, 36, 37]. It is now commonly agreed that the SSE results from the thermal generation of magnon spin currents in the FM and electrically converted by the ISHE in the NM [43, 44, 45, 46, 65, 115]. Usually the FM insulator is treated as a conventional ferromagnet with a net magnetization, despite its ferri-magnetic nature, with more than one magnetically ordered sublattice [116, 117].

One example of the observation of the multiple magnetic sublattice nature of a ferrimagnet by the SSE, is illustrated by measurements in Gd$_3$Fe$_5$O$_{12}$ [111], a compensated ferrimagnetic oxide with a magnetic compensation point at a temperature of around T_c ~ 288 K [118]. In this system, the SSE shows a sign reversal as the temperature is decreased across the magnetic compensation point (T_c), demonstrating the dependence of the SSE on the individual magnetization of the sublattices of the ferrimagnet, in agreement with theoretical predictions [56]. Furthermore, as the temperature is further reduced an additional sign reversal was observed, which was explained as a consequence of the spin current induced by higher-energy magnon modes of the material, proving the dependence of the SSE on the complex spin wave dynamics in ferrimagnets [111].

The dependence of the SSE on the details of the spin wave spectrum has been further demonstrated by

measurements of the SSE in antiferromagnetically ordered materials [50, 51]. In these materials two equivalent sublattices with opposite spin polarizations are present, giving rise to two overlapping spin wave dispersions with opposite spin polarizations, application of a relatively strong field can split these spin wave modes, where the frequency of the modes is increased/decreased depending on the relative orientation of the spin polarization with the applied magnetic field, and results in the generation of a net spin current [52]. This antiferromagnetic-spin-wave-driven SSE has been experimentally demonstrated for Cr_2O_3 [50] and MnF_2 [51], these studies also report the observation of a characteristic spin-flop induced voltage when a large magnetic field is applied along the crystalline easy axis of the antiferromagnet, thus demonstrating the antiferromagnetic origin of the observed signal.

Common SSE theories rely on long-range magnetically ordered materials, however recent studies show the existence of a SSE in insulating paramagnetic oxides [112] and magnetically frustrated systems (one-dimensional spin-1/2 chains) [113], where no long-range magnetic order is present. The observed SSE is understood as a result of short ranged magnetic correlations which can drive spin currents, however the origin of the SSE in paramagnets and one-dimensional spin-1/2 chain systems is fundamentally different, being driven by a spinon spin current in the latter case [113]. In light of the above, it is also interesting to mention the recent observation of a spin-transport in an amorphous magnetic insulator [114]. The SSE was also previously observed in a non-magnetic semiconductor [119] at low temperatures and high magnetic fields, however its origin is fundamentally different from the SSE phenomena discussed here.

Another parameter that can be tuned in the SSE is the materials used for electrical detection of the thermally generated spin current by the ISHE, where Pt is the most commonly used material, as the spin current detection efficiency is relatively large in this metal [33, 34]. Recently, the ISHE has also been investigated in antiferromagnetic [120, 121, 122] and ferromagnetic metals [105, 106, 107, 123, 124, 125, 126, 127], these studies open the possibility to explore a wider range of materials which are fundamentally interesting and can also possibly lead to increased thermoelectric conversion efficiency of SSE devices, due to combined thermoelectric generation by means of the SSE and ANE.

7. **Summary and outlook.**

We have investigated thermo-spin effects in Fe-oxide based heterostructures. We have mainly focused on the results of the thermos-spin conversion in multilayers formed by repeated growth of FM/NM bilayers, particularly $[Fe_3O_4/Pt]_n$-based systems. Measurements of the SSE and SPE in such multilayer systems present a strong enhancement of the thermoelectric conversion response; this enhancement cannot be simply explained by the system geometry, but other factors need to be taken in consideration. Basically, the propagation of the spin current in the multilayer geometry allows for an enhancement of the spin current in the middle layers of the multilayer structure, due to the continuity and non-zero value of the spin current in the inner interfaces of the multilayer.

We have shown the results on the thermoelectric response of spin Hall thermopiles and multilayer systems: in the former case the sensitivity is increase at the expense of a device resistance increase, resulting in no improvement in the deliverable thermoelectric power. However, the multilayer system with a simultaneous increase in the thermoelectric response and reduction of device internal resistance, was shown to improve the deliverable thermoelectric power on an external resistive load, reaching two orders of magnitude increase with respect to a single bilayer structure. This represents a significant leap in the thermoelectric efficiency of the SSE and SPE. Moreover, the observed multilayer SSE

enhancement is expected to further improve by selection of materials with better spin transport characteristics.

Finally, we also summarize recent results of the SSE in materials with types of magnetic order other than conventional ferro-/ferri- magnetic systems. These can enrich the physical understanding of the thermo-spin effects, span spin-current studies in other areas [128, 129, 130], and possibly provide novel routes of exploration to improve the efficiency of SSE-thermoelectric conversion.

References

[1] Callen H B 1985 *Thermodynamics and an introduction to thermostatistics* (John Wiley & Sons, Inc)

[2] He J and Tritt T M 2017 *Science* **357** 1369

[3] Bauer G E W, Saitoh E and van Wees B J 2012 *Nature Mater.* **11** 391

[4] Boona S R, Myers R C and Heremans J P 2014 *Energy Environ. Sci.* **7** 885

[5] Maekawa S, Adachi H, Uchida K, Ieda J and Saitoh E 2013 *J. Phys. Soc. Japan* **82** 102002

[6] Maekawa S, Saitoh E, Valenzuela S O and Kimura T 2012 *Spin Current* (Oxford, Oxford University Press)

[7] Uchida K *et al.* 2010 *Nature Mater.* **9** 894

[8] Kajiwara Y *et al.* 2010 *Nature* **464** 262

[9] Saitoh E, Ueda M, Miyajima H and Tatara G 2006 *Appl. Phys. Lett.* **88** 182509

[10] Tserkovnyak Y, Brataas A, Bauer G E W and Halperin B I 2005 *Rev. Mod. Phys.* **77** 1375

[11] Uchida K, Takahashi S, Harii K, Ieda J, Koshibae W, Ando K, Maekawa S and Saitoh E 2008 *Nature* **455**, 778

[12] Uchida K, Ishida M, Kikkawa T, Kirihara A, Murakami T and Saitoh E 2016 *Proc. IEEE* **104** 1946

[13] Uchida K, Ishida M, Kikkawa T, Kirihara A, Murakami T and Saitoh E 2014 *J. Phys.: Condens. Matter* **26** 343202

[14] Uchida K, Adachi H, An T, Ota T, Toda M, Hillebrands B, Maekawa S and Saitoh E 2011 *Nature Mater.* **10** 737

[15] Uchida K, Adachi H, An T, Nakayama H, Toda M, Hillebrands B, Maekawa S and Saitoh E 2012 *J. Appl. Phys.* **111** 053903

[16] Weiler M, Huebl H, Goerg F S, Czeschka F D, Gross R and Goennenwein S T B 2012 *Phys. Rev. Lett.* **108** 176601

[17] Azevedo A, Vilela Leão L H, Oliveira A B and Rezende S M 2005 *J. Appl. Phys.* **97** 10C715

[18] Costache M V, Sladkov M, Watts S M, van der Wal C H and van Wees B J 2006 *Phys. Rev. Lett.* **97** 216603

[19] Valenzuela S O and Tinkham M 2006 *Nature* **442** 176

[20] Kimura T, Otani Y, Sato T, Takahashi S and Maekawa S 2007 *Phys. Rev. Lett.* **98** 156601

[21] Flipse J, Dejene F K, Wagenaar D, Bauer G E W, Ben Youssef J and van Wees B J 2016 *Phys. Rev. Lett.* **113** 027601

[22] Daimon S, Iguchi R, Hioki T, Saitoh E and Uchida K 2016 *Nat. Commun.* **7**, 13754

[23] Uchida K *et al.* 2017 *Phys. Rev. B* **95** 184437

[24] Daimon S, Uchida K, Iguchi R, Hioki T and Saitoh E 2017 *Phys. Rev. B* **96** 024424

[25] Itoh R, Iguchi R, Daimon S, Oyanagi K, Uchida K and Saitoh E 2017 *Phys. Rev. B* **96** 184422

[26] Grau-Crespo R, Al-Baitai A Y, Saadoune I and De Leeuw N H 2010 *J. Phys. Condens. Matter* **22** 255401

[27] Dronskowski R 2001 *Adv. Funct. Mater.* **11** 27

[28] Walz F 2002 *J. Phys.: Condens. Matter* **14** R285

[29] Jin X S, Ramos R, Zhou Y, McEvoy C and Shvets I V 2006 **99** 08C509

[30] Ramos R, Arora S K and Shvets I V 2008 *Phys. Rev. B* **78** 214402

[31]Fernández-Pacheco A, De Teresa J M, Orna J, Morellón L, Algarabel P A, Pardo J A and Ibarra M R 2008 *Phys. Rev. B* **77**, 100403

[32] Wu H C, Ramos R, Sofin R G S, Liao Z M, Abid M and Shvets I V 2012 *Appl. Phys. Lett.* **101** 052402

[33] Hoffmann A 2013 *IEEE Trans. Magn.* **49** 5172

[34] Sinova J, Valenzuela S O, Wunderlich J, Back C H and Jungwirth T 2015 *Rev. Mod. Phys.* **87** 1213

[35] Xiao J, Bauer G E W, Uchida K, Saioth E and Maekawa S 2010 *Phys. Rev. B* **81** 214418

[36] Adachi H, Ohe J, Takahashi S and Maekawa S 2011 *Phys. Rev. B* **83** 094410

[37] Adachi H, Uchida K, Saitoh E and Maekawa S 2013 *Rep. Prog. Phys.* **76** 36501

[38] Kehlberger *et al.* 2015 *Phys. Rev. Lett.* **115** 096602

[39] Kikkawa T, Uchida K, Daimon S, Qiu Z, Shiomi Y and Saitoh E 2015 *Phys. Rev. B* **92** 064413

[40] Kikkawa T *et al.* 2013 *Phys. Rev. B* **88** 214403

[41] Jin H, Boona S R, Yang Z, Myers R C and Heremans J P 2015 *Phys. Rev. B* **92** 054436

[42] Ritzmann U, Hinzke D, Kehlberger A, Guo E-J, Kláui M and Nowak U 2015 *Phys. Rev. B* **92** 174411

[43] Rezende S M, Rodríguez-Suárez R L, Cunha R O, Rodrigues A R, Machado F L A, Fonseca Guerra G A, Lopez Ortiz J C and Azevedo A 2014 *Phys. Rev. B* **89** 014416

[44] Rezende S M, Rodríguez-Suárez R L, Cunha R O, Lopez Ortiz J C and Azevedo 2016 *J. Magn. Magn. Mater.* **400** 171

[45] Zhang S S-L, and Zhang S 2012 *Phys. Rev. Lett.* **109**, 096603

[46] Zhang S S-L, and Zhang S 2012 *Phys. Rev. B* **86**, 214424

[47] Ramos R *et al.* 2015 *Phys. Rev. B* **92** 220407(R)

[48] Ramos R, Anadón A, Lucas I, Uchida K, Algarabel P A, Morellón L, Aguirre M H, Saitoh and Ibarra M R 2016 *APL Mater.* **4** 104802

[49] Ramos R *et al.* 2017 *AIP Advances* **7** 055915

[50] Seki S, Ideue T, Kubota M, Kozuka Y, Takagi R, Nakamura M, Kaneko Y, Kawasaki M and Tokura Y 2015 *Phys. Rev. Lett.* **115** 266601

[51] Wu S M, Zhang W, KC A, Borisov P, Pearson J E, Jiang J S, Lederman D, Hoffmann A and Bhattacharya A 2016 *Phys. Rev. Lett* **116** 097204

[52] Rezende S M and Rodríguez-Suárez R L 2015 *Phys. Rev. B* **93** 014425

[53] Rezende S M and Rodríguez-Suárez R L 2016 *Phys. Rev. B* **93** 054412

[54] Ohe J, Adachi H, Takahashi S and Maekawa S 2011 *Phys. Rev. B* **83** 115118

[55] Bender S A, Duine R A and Tserkovnyak 2012 *Phys. Rev. Lett.* **108** 246601

[56] Ohnuma Y, Adachi H, Saitoh E and Maekawa S 2013 *Phys. Rev. B* **87** 014423

[57] Chotorlishvili L, Toklikishvili Z, Dugaev V K, Barnaś J, Trimper S and Berakdar J 2013 *Phys. Rev. B* **88** 144429

[58] Ren J 2013 *Phys. Rev. B* **88** 220406

[59] Bender S A and Tserkovnyak 2015 *Phys. Rev. B* **91** 140402

[60] Lyapilin I I, Okorokov M S and Ustinov V V 2015 *Phys. Rev. B* **91** 195309

[61] Etesami S R, Chotorlishvili L and Berakdar J 2015 *Appl. Phys. Lett.* **107** 132402

[62] Brataas A, Skarsvåg H, Tveten E G and Fjaerbu E L 2015 *Phys. Rev. B* **92** 180414

[63] Chotorlishvili L, Toklikishvili Z, Etesami S R, Dugaev V K, Barnaś J and Berakdar J 2015 *J. Magn. Magn. Mater.* **396** 254

[64] Tserkovnyak Y, Bender S A, Duine R A and Flebus B 2016 *Phys. Rev. B* **93** 100402(R)

[65] Cornelissen L J, Peters K J H, Bauer G E W, Duine R A and van Wees BJ 2016 *Phys. Rev. B* **94** 014412

[66] Scharf B, Matos-Abiague A, Žutic I and Fabian J 2012 *Phys. Rev. B* **85** 085208

[67] Adachi H, Uchida K, Saitoh E, Ohe J, Takahashi S and Maekawa S 2010 *Appl. Phys. Lett.* **97** 252506

[68] Tikhonov K S, Sinova J and Finkel'stein A M 2013 *Nat. Commun.* **4** 1945

[69] Bosu S, Sakuraba Y, Uchida K, Saito K, Ota T, Saitoh E and Takanashi K 2011 *Phys. Rev. B* **83** 224401

[70] Jaworski C M, Yang J, Mack S, Awschalom D D, Heremans J P and Myers R C 2010 *Nature Mater.* **9**, 898

[71] Arboleda J D, Olmos O A, Aguirre M H, Ramos R, Anadón A and Ibarra M R 2016 *Appl. Phys. Lett.* **108** 232401

[72] Meier D *et al.* 2015 *Nature Commun.* **6** 8211

[73] Bosu S, Sakuraba Y, Uchida K, Saito K, Kobayashi W, Saitoh E and Takanashi K 2012 *J. Appl. Phys.* **111** 07B106

[74] Wang S H, Zou L K, Cai J W, Shen B G and Sun J R 2013 *Phys. Rev. B* **88** 214304

[75] Schmid M, Srichandan S, Meier D, Kuschel T, Schmalhorst J-M, Vogel M, Reiss G, Strunk C and Back C H 2013 *Phys. Rev. Lett.* **111** 187201

[76] Giles B L, Yang Z, Jamison J S and Myers R C 2015 *Phys. Rev. B* **92** 224415

[77] Ganzhorn K *et al.* 2017 *AIP Advances* **7** 085102

[78] Cornelissen L J, Oyanagi K, Kikkawa T, Qiu Z, Kuschel T, Bauer G E W, van Wees B J and Saitoh E 2017 *Phys. Rev. B* **96** 104441
[79] Weiler M *et al.* 2012 *Phys. Rev. Lett.* **108** 106602
[80] Lee W-L, Watauchi S, Miller V L, Cava R J and Ong N P 2004 *Phys. Rev. Lett.* **93** 226601
[81] Miyasato T, Abe N, Fujii T, Asamitsu A, Onoda S, Onose Y, Nagaosa N and Tokura Y 2007 *Phys. Rev. Lett.* **99** 086602
[82] Pu Y, Chiba D, Matsukura F, Ohno H and Shi J 2008 *Phys. Rev. Lett.* **101** 117208
[83] Mizuguchi M, Ohata S, Uchida K, Saitoh E and Takanashi K 2012 *Appl Phys. Express* **5** 093002
[84] Ramos R *et al.* 2014 *Phys. Rev. B* **90** 054422
[85] Fang C, Wan C H, Yuan Z H, Huang L, Zhang X, Wu H, Zhang Q T and Hou X F 2016 *Phys. Rev. B* **93** 054420
[86] Ramos R *et al.* 2013 *Appl. Phys. Lett.* **102** 072413
[87] Basso V, Ferraro E, Magni A, Sola A, Kuerpferling M and Pasquale M 2016 *Phys. Rev. B* **93** 184421
[88] Basso V, Ferraro E and Piazzi M 2016 *Phys. Rev. B* **94** 144422
[89] Ohnuma T, Matsuo M and Maekawa S 2017 *Phys. Rev. B* **96** 134412
[90] Breitenstein O, Warta W and Langenkamp M 2010 *Lock-in Thermography: Basics and Use for Evaluating Electronic Devices and Materials* (Berlin: Springer)
[91] Wid O, Bauer J, Muller A, Breitenstein, Parkin S S P and Schmid G 2016 *Sci. Rep.* **6** 28233
[92] Jiménez-Cavero P *et al.* 2017 *APL Mater.* **5** 026103
[93] Anadón A, Ramos R, Lucas I, Algarabel P A, Morellón L, Ibarra M R and Aguirre M H 2016 *Appl. Phys. Lett.* **109** 012404
[94] Uchida K, Kikkawa T, Seki T, Oyake T, Shiomi J, Qiu Z, Takanashi K and Saitoh E 2015 *Phys. Rev. B* **92** 094414
[95] Lee K-D *et al.* 2015 *Sci. Rep.* **5** 10249
[96] Boona S R, Vandaele K, Boona I N, McComb D W and Heremans J P 2016 *Nat. Commun.* **7** 13714
[97] Shiomi Y, Handa Y, Kikkawa T and Saitoh E 2015 *Appl. Phys. Lett.* **106** 232403
[98] Takahashi S, Saitoh E and Maekawa S 2010 *J. Phys.: Conf. Ser.* **200** 062030
[99] Kirihara A, Uchida K, Kajiwara Y, Ishida M, Nakamura Y, Manako T, Saitoh E and Yorozu S 2012 *Nat. Mater.* **11** 686
[100] Kirihara A *et al.* 2016 *Sci. Rep.* **6** 23114
[101] Liu L, Pai C-F, Li Y, Tseng H W, Ralph D C and Buhrman R A 2012 *Science* **336** 555
[102] Niimi Y, Kawanishi Y, Wei D H, Deranlot C, Yang H X, Chshiev M, Valet T, Fert A and Otani Y 2012 *Phys. Rev. Lett.* **109** 156602
[103] Laczkowski P *et al.* 2014 *Appl. Phys. Lett.* **104** 142403
[104] Jiang Z, Chang C-Z, Masir M R, Tang C, Xu Y, Moodera J S, MacDonald A H and Shi J 2016 *Nat. Commun.* **7** 11458
[105] Okuma N, Masir M R and MacDonald A H 2017 *Phys. Rev. B* **95** 165418
[106] Kikkawa T, Uchida K, Daimon S, Shiomi Y, Adachi H, Qiu Z, Hou D, Jin X-F, Maekawa S and Saitoh E 2013 *Phys. Rev. B* **88** 214403
[107] Miao B F, Huang S Y, Qu D and Chien C L 2013 *Phys. Rev. Lett.* **111** 066602
[108] Tian D, Li Y, Qu D, Jin X and Chien C L 2015 *Appl. Phys. Lett.* **106** 212407
[109] Uchida K, Nonaka T, Yoshino T, Kikkawa T, Kikuchi D and Saitoh E 2012 *Appl. Phys. Express* **5** 093001
[110] Sagasta E, Omori Y, Isasa M, Gradhand M, Hueso L E, Niimi Y, Otani Y and Casanova F 2016 *Phys. Rev. B* **94** 060412
[111] Geprägs S *et al.* 2016 *Nat. Commun.* **7** 10452
[112] Wu S M, Pearson J E and Bhattacharya 2015 *Phys. Rev. Lett.* **114** 186602
[113] Hirobe D, Sato M, Kawamata T, Siomi Y, Uchida K, Iguchi R, Koike Y, Maekawa S and Saitoh E 2017 *Nature Phys.* **13** 30
[114] Wesenberg D, Liu T, Balzar D, Wu M and Zink B L 2017 *Nature Phys.* **13** 987
[115] Kikkawa T, Shen K, Flebus B, Duine R A, Uchida K, Qiu Z, Bauer G E W and Saitoh E 2016 *Phys. Rev. Lett.* **117** 207203

[116] Barker J and Bauer G E W 2016 *Phys. Rev. Lett.* **117** 217201

[117] Princep A J, Ewings R A, Ward S, Tóth S, Dubs C, Prabhakaran D and Boothroyd A T 2017 *npj Quantum Materials* **2** 63

[118] Pauthenet R. 1958 *J. Appl. Phys.* **29** 253

[119] Jaworski C M, Myers R C, Johnston-Halperin and Heremans J P 2012 *Nature* **487** 210

[120] Frangou L, Oyarzún S, Auffret S, Vila L, Gambarelli S and Baltz V 2016 *Phys. Rev. Lett.* **116** 077203

[121] Zhang W, Jungfleisch M B, Jiang W, Pearson J E and Hoffmann A 2014 *Phys. Rev. Lett.* **113** 196602

[122] Zu D, Huang S Y and Chien C L 2015 *Phys. Rev. B* **92** 020418

[123] Azevedo A, Alves Santos O, Fonseca Guerra G A, Cunha R O, Rodríguez-Suárez R and Rezende S M 2014 *Appl. Phys. Lett.* **104** 052402

[124] Wu S M, Hoffmann J, Pearson J E and Bhattacharya A 2014 *Appl. Phys. Lett.* **105** 092409

[125] Du C, Wang H, Yang F and Hammel P C 2014 *Phys. Rev. B* **90** 140407

[126] Seki T, Uchida K, Kikkawa T, Qiu Z and Saitoh E 2015 *Appl. Phys. Lett.* **107** 092401

[127] Ramos R, Wongjom P, Iguchi R, Yagmur A, Qiu Z, Pinitsoontorn S, Uchida K and Saitoh E 2018 *J. Magn. Magn. Mater.* **447** 134

[128] Walowski J and Münzenberg M 2016 *J. Appl. Phys.* **120** 140901

[129] Seifert T *et al.* 2017 *Spin* **7** 1740010

[130] Seifert T *et al.* 2017 arXiv:1709.00768 [cond-mat.mes-hall]